Main-Reflector Shaping of Omnidirectional Dual Reflectors Using Local Conic Sections

Rafael A. Penchel, José R. Bergmann, and Fernando J. S. Moreira

***Abstract*—This work presents an alternative method for GO synthesis of dual-reflector antennas suited for omnidirectional coverage. Both reflectors are bodies-of-revolution where a single conic section generates the sub-reflector while a concatenation of local conic sections represent the main-reflector generatrix, which is shaped to provide an arbitrary radiation pattern in the antenna's elevation plane. To illustrate the method, omnidirectional axis-displaced ellipse (OADE) configurations are synthesized to provide a cosecant squared radiation pattern in the elevation plane. Two different ray structures are considered: with real or virtual main-reflector caustics. The GO shaping results are validated by method-of-moments simulations.**

***Index Terms*—Omnidirectional radiation pattern, reflector antenna, reflector shaping.**

I. Introduction

At microwave and millimeter-wave frequencies, omnidirectional single and dual reflector antennas may lead to designs which can be employed in hub stations. Several design examples are found in the literature [1]–[3], where the reflector surfaces are bodies of revolution (BORs), as illustrated in Fig. 1. The shape of the surfaces generatrices controls the antenna radiation pattern in the vertical (elevation) plane. The use of reflector antennas allows the control of the radiation pattern, perhaps with very low sidelobe levels, in tradeoff of antenna size and complexity.

Several studies have dealt with the shaping of circularly symmetric dual-reflector antennas by solving an ordinary differential equation derived from Geometrical Optics (GO) principles [1], [3], [4]. An alternative shaping technique for circularly symmetric dual reflectors was implemented by combining local conventional dual-reflector systems and imposing simple ray tracing, leading to an iterative solution of nonlinear algebraic equations to obtain the shaped reflector surfaces [5]. The technique was further improved by using polar coordinates to describe the local conic sections, leading to a one-step procedure requiring the solution of simple linear algebraic equations [6]. The algorithm of [6] was suited to shape omnidirectional dual-reflector configurations [7]. It was demonstrated that the shaping algorithms based on the concatenation of local conic sections have higher convergence rates than traditional methods based on the numerical evaluation of ordinary differential equations [6], [7].

In [7] the antenna radiation pattern in the elevation plane was controlled by shaping both sub-and main-reflectors. Alternative configurations may have a classical sub-reflector (i.e., a BOR sub-reflector generated by a single axis-displaced conic section) and a shaped main reflector. Omnidirectional dual-reflector configurations with only the main reflector shaped were investigated in [8], [9]. In the present work, the studies conducted in [8], [9] are extended by investigating two different ways of specifying the local conic sections that represent the shaped main-reflector generatrix: the combination of local hyperbolas and ellipses (Method I), which ensures the continuity of the generatrix and its first-order derivative; and the combination of local parabolas (Method II), which only ensures the continuity of the generatrix, but yields a simpler set of equations to be solved. Both methods lead to one-step iterative procedures with simple algebraic equations to be evaluated. To illustrate the technique we consider omnidirectional axis-displaced ellipse (OADE) configurations where the sub-reflector generatrix is an axis-displaced ellipse and the main-reflector shaping generates a cosecant squared radiation pattern in the elevation plane. The convergence rates of Methods I and II are explored and compared with results provided by a technique based on the solution of an ordinary differential equation (Method III) [10]. To evaluate the synthesized radiation patterns, the solution of an electric field integral equation via method of moments (MoM) is employed [11].

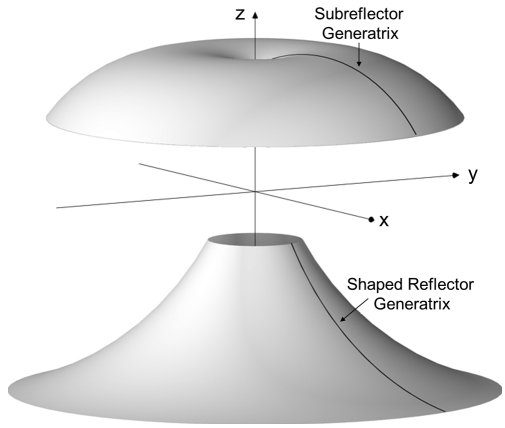

Fig. 1. Circularly symmetric dual-reflector surfaces.

II. Main-Reflector Shaping by Conic Section: Method I

The OADE antennas investigated are composed of two surfaces of revolution with a common axis of symmetry (z-axis). The sub-reflector generatrix is an axis-displaced ellipse with two foci: one located at the origin (O) and another (P) placed away from the symmetry axis, as illustrated in Fig. 2. The feed phase center is at O while P defines a real circular caustic between the reflectors. The sub-reflector is illuminated by a point source at O with circularly symmetric radiation pattern $G_F(\theta_F)$, where θ_F defines the feed-ray direction relative to the z-axis. After reflection at the sub-reflector, the ray crosses the caustic P with an angle θ_S before being reflected by the main reflector (Fig. 2). The main reflector is shaped to radiate a prescribed vertical pattern $G_A(\theta)$ in the far-field region of the antenna, where θ is the direction of observation relative to the z-axis and $\theta \in [\theta_0, \theta_n]$ defines the tube of rays reflected by the main reflector. The ellipse that generates the sub-reflector surface is established from the values desired for the distances V_S and z_B, diameters D_S and D_B and for the edge angle θ_E (see Fig. 2) with the help of the formulation presented in Section III of [10]. From the ellipse polar equation, one obtains the useful relation between θ_S and θ_F [10]:

$$\cot\left(\frac{\theta_S}{2}\right) = \frac{\varepsilon\cos\beta + 1 - \varepsilon\sin\beta\cot(\theta_F/2)}{\varepsilon\sin\beta + (\varepsilon\cos\beta - 1)\cot(\theta_F/2)} \tag{1}$$

Manuscript received July 03, 2012; revised March 29, 2013; accepted April 22, 2013. Date of publication May 03, 2013; date of current version July 31, 2013. This work was partially supported by CNPq, CAPES, and FAPEMIG, Brazil.

R. A. Penchel and J. R. Bergmann are with the Center for Telecommunication Studies, Pontifical Catholic University of Rio de Janeiro, Rio de Janeiro, RJ 22451-900, Brazil (e-mail: rapenchel@cetuc.puc-rio.br; bergmann@cetuc.puc-rio.br).

F. J. S. Moreira is with the Department of Electronics Engineering, Federal University of Minas Gerais, Belo Horizonte, MG 31270-970, Brazil. (e-mail: fernandomoreira@ufmg.br).

Digital Object Identifier 10.1109/TAP.2013.2261571

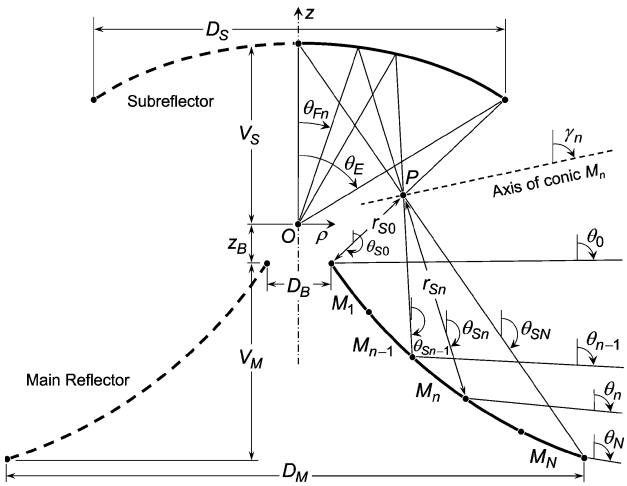

Fig. 2. Basic geometric parameters of an OADE antenna with shaped main reflector.

where ϵ is the eccentricity and β is the axial tilt angle of the ellipse.

In Method I, the shaped main-reflector generatrix is represented by a combination of local conic sections $M_n (n = 1, \ldots, N$, as illustrated in Fig. 2), sequentially concatenated to each other and all of them with one of their foci at P. The conic section M_n is limited by angles θ_{Sn-1} and θ_{Sn} and its axis has an elevation (tilt) angle γ_n with respect to the z-axis. r_S is the distance between P and a point at M_n and is given by:

$$r_S = \frac{a_n}{b_n \sin\theta_S + (1+d_n)\cos\theta_S - 1}, \text{for } \theta_S \in [\theta_{Sn-1}, \theta_{Sn}] \quad (2)$$

where

$$a_n = c_n\,(e_n - 1/e_n) \quad (3)$$

$$b_n = e_n \sin\gamma_n \quad (4)$$

$$d_n = e_n \cos\gamma_n - 1 \quad (5)$$

and $2c_n$ and e_n are the inter-focal and eccentricity of M_n, respectively. Consequently, M_n is defined after a_n, b_n, and d_n are determined. Each conic section M_n is sequentially defined by the following iterative procedure.

The feed angle θ_F is decreasingly varied from θ_E to 0, with $\theta_{Fn-1} - \theta_{Fn} = \Delta\theta = \theta_E/N$. Observe that the ray-trajectory directions θ_{Sn} and θ_n are related to θ_{Fn} (Fig. 2). The initial parameters $(n = 0)$ are determined from the positions of the sub-reflector edge and of the main-reflector central opening, located by the parameters V_S, z_B, D_S, D_B, and θ_E previously used to specify the sub-reflector. For $n = 1, \ldots, N$, the conic M_n is determined as follows. From (2) and the values of r_{Sn-1} and θ_{Sn-1} determined in the previous step $(n-1)$ one obtains:

$$r_{Sn-1} = \frac{a_n}{b_n \sin\theta_{Sn-1} + (1+d_n)\cos\theta_{Sn-1} - 1}. \quad (6)$$

From the polar equation of M_n and the parameters determined in the previous step, one derives the relation between the incident and reflected directions of the ray $(n-1)$:

$$b_n\left[\cot\left(\frac{\theta_{n-1}}{2}\right) + \cot\left(\frac{\theta_{Sn-1}}{2}\right)\right] + d_n\left[\cot\left(\frac{\theta_{n-1}}{2}\right)\cot\left(\frac{\theta_{Sn-1}}{2}\right) - 1\right] = 2. \quad (7)$$

Applying the conservation of energy to the tube of rays departing from O, one obtains a relation between θ_F and θ:

$$\int_{\theta_{Fn}}^{\theta_E} G_F(\theta_F)\sin\theta_F d\theta_F = N_F \int_{\theta_0}^{\theta_n} G_A(\theta)\sin\theta d\theta \quad (8)$$

where the normalization constant N_F ensures that the power inside the tube of rays departing from O remains the same after reflection at the main reflector, while θ_0 is the prescribed direction of the ray reflected by the main reflector at step $n = 0$ (Fig. 2). The relation between the prescribed far-field directions θ_0 and θ_n define the characteristic of the main-reflector caustic in the elevation plane. If $\theta_n > \theta_0$ the caustic is virtual, as depicted in Fig. 2. Otherwise, the caustic is real (i.e., the rays intercept each other after reflection at the main reflector). After calculating θ_{Sn} and θ_n from (1) and (8), respectively, one can rewrite (7) for the other extreme point of M_n as follows:

$$b_n\left[\cot\left(\frac{\theta_n}{2}\right) + \cot\left(\frac{\theta_{Sn}}{2}\right)\right] + d_n\left[\cot\left(\frac{\theta_n}{2}\right)\cot\left(\frac{\theta_{Sn}}{2}\right) - 1\right] = 2. \quad (9)$$

Equation (6), (7), and (9) form a set of three linear equations from where the parameters a_n, b_n, and d_n (and, consequently c_n, e_n, and γ_n) are calculated, thus determining the main-reflector local conic section M_n. It is important to observe that, as a given ray trajectory "$n-1$" is reflected by both M_{n-1} and M_n at the same direction (see Fig. 2), Snell's law guarantees that the main-reflector generatrix and its first-order derivative are both continuous. The formulation can be suited to accommodate different antenna configurations. For example, formulas for an omnidirectional axis-displaced Cassegrain (OADC) are presented in [8].

III. Main-Reflector Shaping by Local Parabolas: Method II

In Method II, parabolas are used instead of ellipses or hyperbolas to locally describe the shaped main-reflector generatrix. The procedure is similar to that described in Section II, except as follows. To describe each parabola section M_n, one can use (2–5), with $a_n = -2F_n$ and $e_n = 1$, where F_n is the focal length of parabola M_n. All parabolas share the same focus P. As the eccentricity $e_n = 1$, only F_n and γ_n remain to be determined at each step. The angle θ_n of the ray that is reflected by a parabola M_n is equal to the angle γ_n of that parabola's axis. Consequently, in Method II (8) is rewritten as:

$$\int_{\theta_{Fn}}^{\theta_E} G_F(\theta_F)\sin\theta_F d\theta_F = N_F \int_{\theta_0}^{\gamma_n} G_A(\theta)\sin\theta d\theta \quad (10)$$

which provides γ_n at a given step n. With r_{Sn-1} and θ_{Sn-1} determined in the previous step $n-1$, (6) with $a_n = -2F_n$ and $e_n = 1$ can be used to obtain F_n:

$$F_n = \frac{r_{Sn-1}}{2}\left[1 - \cos(\gamma_n - \theta_{Sn-1})\right]. \quad (11)$$

Then, r_{Sn} is calculated for further use in the following step $(n+1)$:

$$r_{Sn} = \frac{2\,F_n}{[1 - \cos(\gamma_n - \theta_{Sn})]}. \quad (12)$$

The procedure is simpler than Method I and yields a continuous generatrix, but with discontinuous derivative at points between consecutive parabolas.

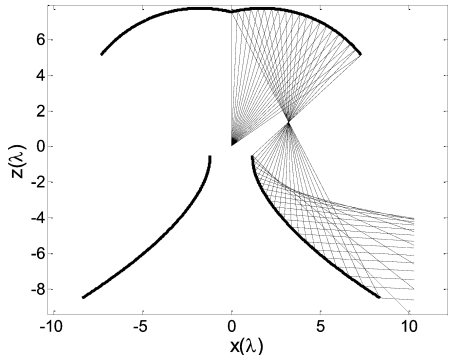

Fig. 3. Shaped antenna with real caustic in front of the main reflector.

IV. Case Studies

To evaluate the shaping procedures described in Sections II and III, we explore two case studies where the main reflector is shaped to generate a cosecant squared radiation pattern $G_A(\theta)$ in elevation plane. For the task, $G_A(\theta)$ is described as:

$$G_A(\theta) = G_{Ao}\csc^2\left(\theta - \frac{\pi}{2}\right), \text{ for } \theta \in [\theta_0, \theta_N] \tag{13}$$

where G_{Ao} is a normalization factor that can be set equal to

$$G_{Ao} = \frac{1}{2\pi}\left|\frac{\cos\theta_0 \cos\theta_N}{\cos\theta_0 - \cos\theta_N}\right| \tag{14}$$

for unity radiated power. Thus, when working with this objective radiation pattern, free-space attenuation is compensated by the higher directivity toward the region farthest from the source, achieving in this way a uniform distribution of power in the coverage area. In this communication, the dual-reflector feed is modeled by a circularly symmetric radiation pattern given by:

$$G_F(\theta_F) = G_{Fo}\left[\frac{J_0(kr_i \sin\theta_F) - J_0(kr_e \sin\theta_F)}{\sin\theta_F}\right]^2, \quad \text{for } \theta_F \le \frac{\pi}{2} \tag{15}$$

where G_{Fo} is a normalization factor. Equation (15) represents the radiation from a coaxial aperture on a perfect electric conductor plane illuminated by its TEM mode, where r_i and r_E are the inner and outer radii, respectively. In both case studies, $r_i = 0.45\ \lambda$ and $r_E = 0.90\ \lambda$.

A. Shaped OADE Antenna With Real Caustic

In the first example, the main reflector was shaped to radiate a cosecant squared pattern between $\theta_0 = 135^\circ$ and $\theta_n = 93^\circ$, with a real caustic in front of the main reflector ($\theta_0 > \theta_n$), as illustrated in Fig. 3. The sub-reflector design follows the procedure described in [10], where the distance between focus O and sub-reflector apex $V_S = 7.54\ \lambda$, main-reflector aperture width $W_A = 7.0\ \lambda$, the main reflector diameter $D_M = 17.56\ \lambda$, the main-reflector central opening is placed at $z_B = -0.5\ \lambda$ with diameter $D_B = 2.4\ \lambda$. These values provide a generating ellipse with eccentricity $\varepsilon = 0.241372$, inter-focal distance $2c = 3.503\ \lambda$, and axial tilt angle $\beta = 67.18^\circ$. Consequently, the sub-reflector has a diameter $D_S = 14.669\ \lambda$ and edge angle $\theta_E = 55.08^\circ$. Table I shows a summary of some relevant dimensions of the shaped antenna. For a comparative study, a reference surface was obtained by employing the synthesis method presented in [10] (Method III) for a very large number of steps ($N = 10^5$).

TABLE I
Some Relevant Dimensions of the Shaped Antennas (Ref. Solution)

Dimensions	OADE with real caustic	OADE with virtual caustic
$D_S(\lambda)$	14.669	14.708
$V_S(\lambda)$	7.540	7.636
$D_M(\lambda)$	16.775	26.824
$V_M(\lambda)$	8.517	17.421
$D_B(\lambda)$	2.40	2.40
$z_B(\lambda)$	–0.50	0
$2c(\lambda)$	3.503	3.603
β	67.18°	62.41°
θ_E	55.08°	54.99°

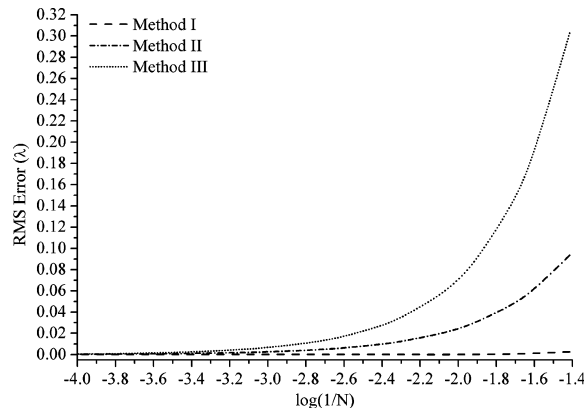

Fig. 4. RMS error of shaped main reflectors with real caustic as function of N.

To illustrate the convergence behavior of the procedures presented in Sections II and III, Fig. 4 shows the RMS error of the shaped main reflector as a function of the number of steps (N) used in the synthesis. For a given value of N, the RMS error was obtained by comparing the distance from P to the shaped main-reflector generatrix along the optical path. As observed from Fig. 4, Method I provides a very small RMS error (smaller than $3\times10^{-3}\ \lambda$) even using $N = 25$ conic sections to represent the shaped main reflector. To achieve similar RMS errors with Methods II and III, it would require $N > 1000$ and $N > 2500$, respectively.

As all methods employ iterative procedures, the error is accumulative and, in general, bigger at the last point (i.e., at the main-reflector edge). For reflectors shaped with 25 steps, Fig. 5 shows the difference (error) between the shaped and the reference surfaces as a function of the reflector's z-coordinate. As observed, for Method I the solution presents errors smaller than $10^{-3}\ \lambda$ at all 25 synthesized points. For Methods II and III the error grows steadily towards the main-reflector edge, being higher for Method III. As Method I also ensures the continuity of the first-order derivative of the reflector surface, it drastically reduces the cumulative error of the numerical solution.

To evaluate the effects of the synthesis error on the antenna radiation pattern, Fig. 6 shows the radiation patterns of the OADE dual-reflector configurations obtained by the three methods, all of them with 25 steps. The reference solution was obtained from Method III with $N = 10^5$. These patterns were simulated by a MoM analysis [11]. During the MoM analysis, the shaped main-reflector generatrices obtained from Methods I and II where described by the corresponding M_n conic sections. For Method III, generatrices are described by straight lines

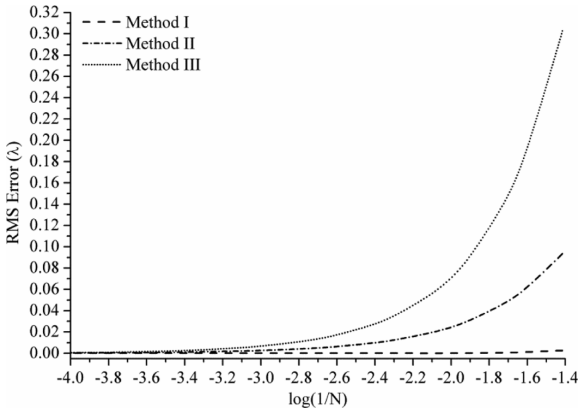

Fig. 5. Error of shaped main reflectors with real caustic as a function of z-coordinate using 25 steps in all syntheses.

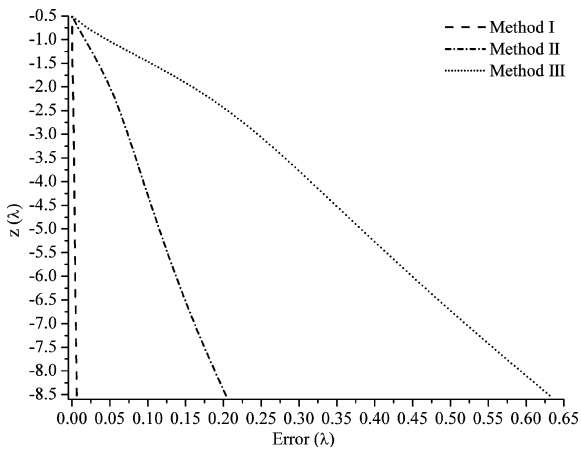

Fig. 6. MoM radiation patterns in the elevation plane of the shaped antennas with real caustic.

uniting synthesized points. As observed in Fig. 6, there are no observable differences between Method I and the reference solutions. Although the shaped surface obtained from Method II is described by only 25 parabolas, the corresponding radiation pattern shows no relevant differences when compared with the one generated from Method I.

B. Shaped OADE Antenna With Virtual Caustic

As an alternative study, the main reflector of the OADE antenna was shaped to present the same radiation pattern, but with a virtual caustic ($\theta_0 = 93^\circ$ and $\theta_N = 135^\circ$), as illustrated in Fig. 7. The other input parameters are those of the previous case, except $V_S = 7.636\ \lambda$ and $z_B = 0$. These values provide a sub-reflector generating ellipse with eccentricity $\varepsilon = 0.250180$, inter-focal distance $2c = 3.603\ \lambda$, and axial tilt angle $\beta = 62.41^\circ$. The BOR sub-reflector has diameter $D_S = 14.708\ \lambda$ and edge angle $\theta_E = 54.99^\circ$. Table I shows a summary of some relevant dimensions of the shaped antenna. Again, a reference surface was obtained by employing Method III [10] with $N = 10^5$. From Figs. 3 and 7 one observes that the main reflector with virtual caustic is longer than that synthesized with a real caustic, as the ray incidence near the surface's edge is almost grazing, pushing the surface downwards.

To illustrate the convergence rates of the three methods, Fig. 8 shows the RMS error of the shaped main reflector as a function of N. The comments already made about the results depicted in Fig. 4 for the real caustic configuration are valid here likewise. The RMS errors in

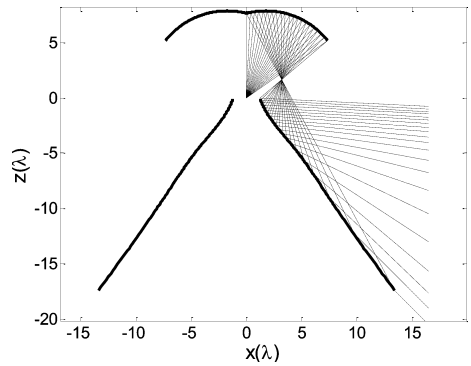

Fig. 7. Shaped antenna with virtual main-reflector caustic.

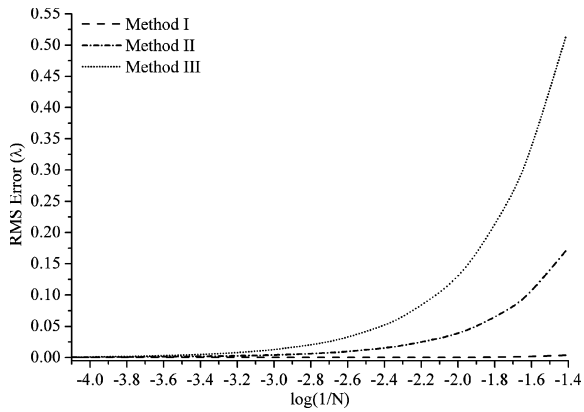

Fig. 8. RMS error of shaped main reflectors with virtual caustic as function of N.

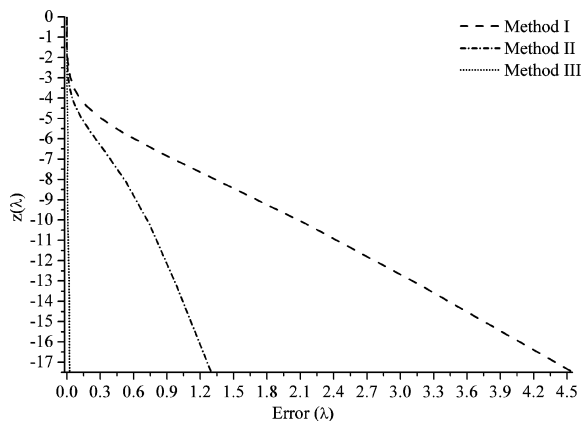

Fig. 9. Error of shaped main reflectors with virtual caustic as a function of z-coordinate using 25 steps in all syntheses.

Fig. 8 are slightly higher than those illustrated in Fig. 4 due to the increase of distance between synthesized points in the longer main reflector with virtual caustic, especially close to its edge. Fig. 9 shows the error between the shaped and the reference surfaces as a function of the reflector's z-coordinate. The comments are basically those already stated for the results presented in Fig. 5. Fig. 10 shows the radiation patterns of the OADE dual-reflector configurations with virtual caustic obtained by the three methods, all of them with 25 steps. The comments are basically those already made with respect to Fig. 6. A comparison between Figs. 6 and 10 indicate that the main-reflector synthesis with a real caustic not only provided a more compact geometry (i.e., a smaller

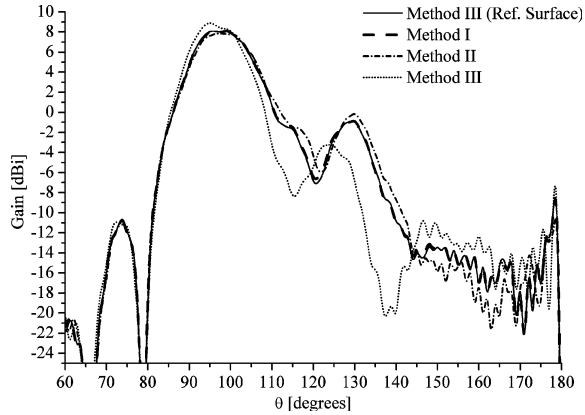

Fig. 10. MoM radiation patterns in the elevation plane of the shaped antennas with virtual caustic.

main reflector) but also most closely fulfilled the cosecant squared radiation spec.

V. Conclusion

This work presented two methods for the main-reflector synthesis of OADE configurations based on GO principles. One method is based on the concatenation of local ellipses and hyperbolas to represent the shaped main-reflector generatrix. In the other method, the conic sections are substituted by parabolas. The former method ensures the continuity of both surface and first-order derivatives. The later method only ensures the surface continuity, but yields simpler equations. As these methods do not solve any differential equation, they are numerically efficient and have higher convergence rates. The shaping procedures were applied in the main-reflector synthesis of OADE configurations, shaped to radiate a cosecant squared pattern. The GO designs were further simulated by MoM analyses.

References

[1] A. Norris and W. Waddoup, "A millimetric wave omnidirectional antenna with prescribed elevation shaping," in *Proc. ICAP 4th Int. Conf. Antennas and Propagation*, 1985, pp. 141–145.

[2] M. Orefice and P. Pirinoli, "Dual reflector antenna with narrow broadside beam for omnidirectional coverage," *Electron. Lett.*, vol. 29, no. 25, pp. 2158–2159, 1993.

[3] A. Pino, A. Acuña, and J. Lopez, "An omnidirectional dual-shaped reflector antenna," *Microw. Opt. Tech. Lett.*, vol. 27, pp. 371–374, 2000.

[4] F. Moreira, A. Prata, Jr., and J. Bergmann, "GO shaping of omnidirectional dual-reflector antennas for a prescribed equi-phase aperture field distribution," *IEEE Trans. Antennas Propag.*, vol. 55, pp. 99–106, 2007.

[5] Y. Kim and T.-H. Lee, "Shaped circularly symmetric dual reflector antennas by combining local conventional dual reflector systems," *IEEE Trans. Antennas Propag.*, vol. 57, no. 1, pp. 47–56, 2009.

[6] F. Moreira and J. Bergmann, "Shaping axis-symmetric dual-reflector antennas by combining conic sections," *IEEE Trans. Antennas Propag.*, vol. 59, no. 3, pp. 1042–1046, 2011.

[7] F. Moreira and J. Bergmann, "Omnidirectional dual-reflector shaping by concatenating conic sections," presented at the 4th Eur. Conf. on Antennas and Propagation (EuCAP 2010), Barcelona, Spain, Apr. 2010.

[8] R. Penchel, J. Bergmann, and F. Moreira, "An omnidirectional dual-reflector antenna with a shaped main reflector described by local conic sections," in *Proc. 5th Eur. Conf. Antennas and Propagation (EuCAP 2011)*, Rome, Italy, Apr. 2011, pp. 1221–1224.

[9] R. Penchel, S. Zang, J. Bergmann, and F. Moreira, "Synthesis and rigorous analysis of omnidirectional ADE antenna with shaped main reflector described by local conic sections," presented at the 6th Eur. Conf. Antennas and Propagation (EuCAP 2012), Prague, Czech Republic, Mar. 2012.

[10] J. Bergmann and F. Moreira, "Omnidirectional ADE antenna with GO shaped main reflector for arbitrary far-field pattern in the elevation plane," *IET Microwaves, Antennas Propag.*, vol. 3, pp. 1028–1035, 2009.

[11] A. Berthon and R. Bills, "Integral equation analysis of radiating structures of revolution," *IEEE Trans. Antennas Propag.*, vol. 37, no. 8, pp. 159–170, 1989.

Compensation of Time-Division Multiplexing Distortion in Switched Antenna Arrays With a Single RF Front-End and Digitizer

S. Henault, B. R. Jackson, and Y. M. M. Antar

***Abstract*—Switched antenna arrays in which a single RF front-end and a single digitizer are used to perform digital array processing are considered in this communication. These arrays offer more simplicity and versatility than time-modulated arrays, and have the advantage of significantly simplifying the design and implementation of smart and MIMO antennas, while minimizing their size, weight, power consumption and cost. They also lend themselves well to an implementation in which a single off-the-shelf software defined radio is used. Unlike previous work where bandwidth was sacrificed to avoid distortion caused by interference between the multiplexed time channels, this work introduces a digital compensation technique that maximizes the system bandwidth and yields performance approaching that of conventional antenna arrays. The technique is demonstrated in various applications, including direction of arrival estimation and beamforming, and can be employed in arrays of other sensor types.**

***Index Terms*—Adaptive arrays, antenna arrays, array signal processing, beam steering, calibration, demultiplexing, direction-of-arrival estimation, error compensation, interference suppression, phased arrays, switched circuits, time division multiplexing.**

I. Introduction

Smart antenna systems offer a variety of interesting applications for civilian and military organizations, including direction of arrival (DOA) estimation, multiple-input-multiple-output (MIMO) operation, digital beamforming and interference suppression [1]. However, these conventional array systems typically require a separate RF front-end and digitizer for each of the array antenna elements, thereby increasing the size, weight, power consumption and cost of the systems, in addition to complicating their design and implementation. To alleviate these problems, it is desirable to implement smart antennas with a single RF

Manuscript received June 18, 2012; revised March 26, 2013; accepted April 18, 2013. Date of publication April 24, 2013; date of current version July 31, 2013.

S. Henault and Y. M. M. Antar are with the Royal Military College of Canada, Electrical and Computer Engineering, Station Forces, Kingston, ON K7K 7B4, Canada (e-mail: henault@ieee.org).

B. R. Jackson is with the Defence Research and Development Canada, Ottawa, ON, Canada.

Color versions of one or more of the figures in this communication are available online at http://ieeexplore.ieee.org.

Digital Object Identifier 10.1109/TAP.2013.2259787